

Article

Vibration Modelling and Control Experiments for a Thin-Walled Cylindrical Rotor with Piezo Patch Actuation and Sensing

Ziv Brand^{1,a}, Matthew O. T. Cole^{1,b,*}, Wichaphon Fakkaew^{2,c}, and Chakkapong Chamroon^{1,d}

¹ Department of Mechanical Engineering, Faculty of Engineering, Chiang Mai University, Chiang Mai, Thailand

² School of Engineering, University of Phayao, Phayao, Thailand

E-mail: ^abrand_ziv@cmu.ac.th, ^bmotcole@dome.eng.cmu.ac.th (Corresponding author), ^cwichaphon.fa@up.ac.th,

^dchakkapong@dome.eng.cmu.ac.th

Abstract. This paper describes a dynamic model formulation and control experiments concerning the vibration behaviour of a thin-walled cylindrical rotor with internal piezoelectric patch transducers. Model development, validation and controller design procedures were undertaken for an experimental rotordynamic system comprising a tubular steel rotor (length 0.8 m, diameter 0.166 m and wall-thickness 3.06 mm) supported by two radial active magnetic bearings. Analytical solutions for mode shapes and natural frequencies for free vibration were first derived using a shell theory model, and these used to construct a speed-dependent parametric model for the rotor structure, including piezo patch actuators and sensors. The results confirm that the developed shell theory model can accurately capture the rotating frame dynamics and accounts correctly for frequency splitting from Coriolis effects. The model is also shown to be suitable for active controller design and optimization. Model-based H_2 feedback control using the rotor-mounted actuators and sensors is shown to achieve vibration suppression of targeted flexural modes, both with and without rotation.

Keywords: Rotordynamics, thin-walled structure, smart structure, optimal control, piezoelectric patch.

ENGINEERING JOURNAL Volume 24 Issue 6

Received 25 March 2020

Accepted 14 September 2020

Published 30 November 2020

Online at <https://engj.org/>

DOI:10.4186/ej.2020.24.6.127

1. Introduction

In rotating machine design, the use of rotors having a hollow thin-walled structure can provide benefits from reduced material usage, low weight and high natural frequencies for beam bending. However, the potential excitation and instability of elastic vibration within the rotor wall must be considered and, if necessary, actively or passively suppressed.

Several previous studies have dealt with bending vibration control using rotor-mounted actuators and sensors. Horst and Wolfel [1] demonstrated a reduction in lateral vibration of a rotating shaft using piezoceramic (PZT) patch actuators bonded to the surface. Finite element modelling and optimal feedback control based on linear quadratic regulation were adopted. Lees and Friswell [2] considered the general problem of strain-based rotor actuation to compensate for imbalance by inducing a rotor bend. Sloetjes and Boer [3] used surface-mounted piezoceramic sheets and strain sensors to control the first bending mode of a helicopter tail drive shaft. Modal control methods were used to suppress resonance and unstable vibration for arbitrary imbalance conditions. Cupial and Koziol [4], [5] examined the compensation of internal damping using piezoelectric patch sensors and actuators fixed to a rotor shaft. Simulation results indicated that the stable speed range could be extended using feedback of the time derivative of the piezo sensor voltage. Przybyłowicz [6] considered the active stabilization of a hollow shaft made with piezoelectric fiber composite. Numerical results with PD feedback of strain values showed that instability caused by internal damping could be mitigated with suitable gain values.

Active vibration control of cylindrical shells has been considered previously for non-rotating structures such as bodies of aircrafts, submarines and rockets/missiles e.g. [7–14]. There have been relatively few studies on active control of rotating shell structures. Kumar and Ray [15] studied the performance of Active Constrained Layer Damping (ACLD) applied to a rotating conical shell. A simple velocity feedback control law was adopted and evaluated by numerical simulation. Model development and experiments on control of circumferential vibration for an annular rotor with magnetic bearing support was presented in [16] and a technique for multi-harmonic vibration suppression proposed in [17]. The optimization of piezo patch actuation and sensing for vibration suppression of a rotating ring was examined in [18] and [19].

This paper considers the active control of circumferential vibration for a thin-walled cylindrical rotor with piezo patch actuators and sensors. A 3-D multi-mode dynamic model based on Love's shell theory [20] is adopted that accounts for the moment distribution from surface mounted piezoelectric actuators under activation. The main contributions from this paper are the model description, its validation, and the experimental results confirming its suitability for optimal

controller design. Accurate account of the effects of rotation distinguish the work from previous studies that consider non-rotating thin-wall cylinders only [11–13].

2. Active Thin-Walled Rotor-Bearing System

An active thin-walled rotor system has been created to enable testing of rotordynamic behaviour and the investigation of different types of vibration control strategies, as shown in Fig. 1. The rotor is supported by two radial active magnetic bearings (AMBs). Piezo patch actuators and sensors can be mounted on the inner surface of the rotor at any position (precluding patch overlap). For the present work, a total of four actuator/sensor pairs were fitted (two pairs at each end of the rotor). The AMBs are a specialized design that employs a distributed actuation scheme to minimize the interaction of the bearing forces with flexural distortion/vibration of the rotor wall [16]. The horizontal rotor has radius 81.5 mm, wall thickness 3.06 mm and axial length 800 mm. The rotor was machined from seamless steel tubing and has the mechanical properties listed in Table 1. The rotor was coupled to a driving disk by four flexible foam polymer straps. This architecture was designed to have minimal effect on the radial dynamics of the rotor. The driving disk was coupled to a brushless dc motor.

The AMBs were operated closed-loop with a control system implemented digitally on PC-based hardware. Current amplifiers (Maxon ESCON 48/5) provided electrical energy to the AMBs, commanded by the control system. Four displacement sensors were used to measure the rotor position for the AMB system. The AMB system provided low stiffness contact-free support of the rotor via the actively controlled magnetic field [21].

Piezoelectric patch actuators and sensors have been mounted internally on the rotor wall for the purpose of stabilization and suppression of flexural vibration occurring within the rotor wall. Laminar composite patch actuators of model P-876A15 from Physik Instrumente were bonded to the inside surface of the cylinder. Four smaller patches (PI P-876SP1) were used as sensors and were glued adjacent to the actuators, as shown in Fig. 2. These patches have polarization in the z-axis direction, giving unimorph mode of operation. Two sensor/actuator pairs (1 and 2) were bonded near to (driven) end A and two sensor/actuator pairs (3 and 4) bonded at end B, as indicated in Table 2. Four piezo driver modules (PI E-835) provided power to the actuators, commanded by a digital control system. All electrical connections to the piezo transducers were through sliprings. The data acquisition, analysis and feedback control algorithms for the piezo-electrics were implemented digitally with PC-based hardware and with a sampling frequency of 8000 Hz.

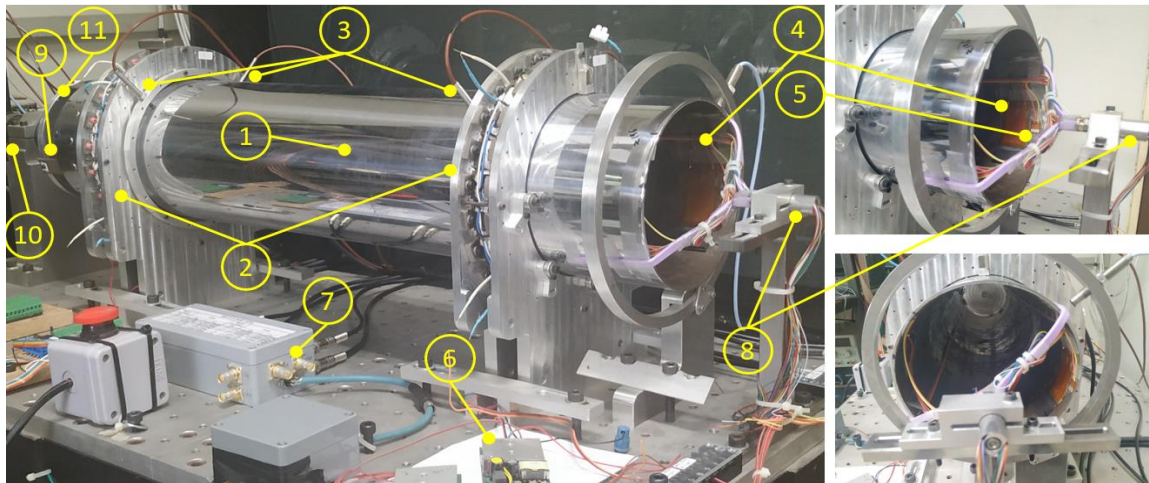


Fig. 1. Experimental active thin-walled rotor system. Main components: 1. steel rotor, 2. radial active magnetic bearings, 3. displacement sensors, 4. piezo patch actuators, 5. piezo patch sensors, 6. piezo driver module, 7. piezo signal conditioning, 8. slip ring, 9. flexure coupling, 10. motor, 11. driving disk.

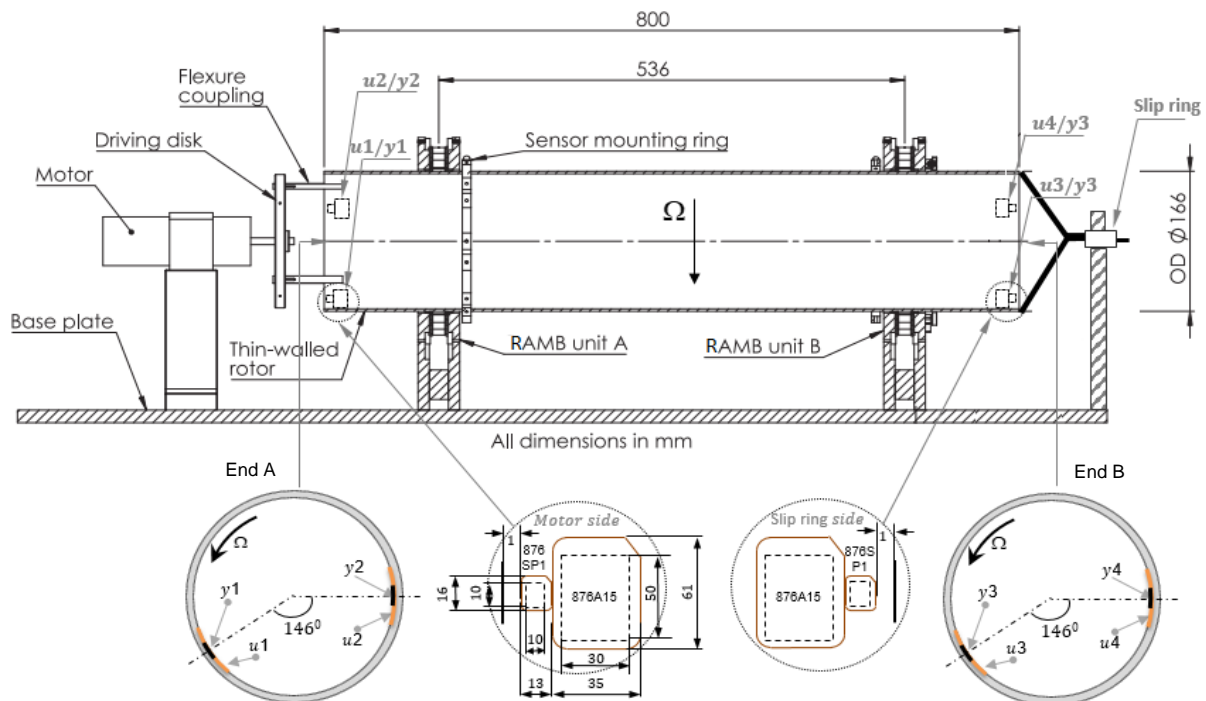


Fig. 2. System cross section showing actuator and sensor patch locations.

Table 1. Rotor properties.

parameter	symbol	value	units
cylinder radius	R	81.5	mm
wall thickness	h	3.06	mm
rotor axial length	L	800	mm
material density	ρ	7850	kg/m ³
Rotor mass		9.61	kg
Young's modulus	E	2.08×10^{11}	N/m ²
Poisson's ratio	ν	0.3	

Table 2. Configuration of piezo patch actuator/sensor pairs.

end	Pair j	type	ϕ_j	z_j (mm)	Input/output signal
A	1	actuator	0°	368.5	u_1
A	1	sensor	0°	392.5	y_1
A	2	actuator	146°	368.5	u_2
A	2	sensor	146°	392.5	y_2
B	3	actuator	0°	-368.5	u_3
B	3	sensor	0°	-392.5	y_3
B	4	actuator	146°	-368.5	u_4
B	4	sensor	146°	-392.5	y_4

Following from Eqs. (1)-(12), a complete description for the shell dynamics is obtained in the form

$$L_x - \frac{h}{2} \left[\frac{K_y}{R^2} \frac{\partial^2 H}{\partial \phi^2} + K_z \frac{\partial^2 H}{\partial z^2} \right] e(t) = \rho h \left[\ddot{u} + 2\Omega \dot{v} - \Omega^2 \left(\frac{\partial^2 u}{\partial \phi^2} + u - \frac{\partial v}{\partial \phi} \right) \right] \quad (13)$$

$$L_y + \frac{h}{2R^2} K_y \frac{\partial H}{\partial \phi} e(t) = \rho h \left[\ddot{v} - 2\Omega \dot{u} + \Omega^2 \left(\frac{\partial u}{\partial \phi} - R \frac{\partial^2 w}{\partial \phi \partial z} \right) \right] \quad (14)$$

$$L_z = \rho h \left[\ddot{w} - \Omega^2 R \frac{\partial^2 w}{\partial \phi^2} \right] \quad (15)$$

where

$$L_x = C \left[\frac{1}{R^2} \frac{\partial v}{\partial \phi} - \frac{u}{R^2} + \frac{v}{R} \frac{\partial w}{\partial z} - D \left[\frac{\partial^4 u}{\partial z^4} + \frac{1}{R^2} \frac{\partial^3 v}{\partial \phi \partial z^2} + \frac{2}{R^2} \frac{\partial^4 u}{\partial \phi^2 \partial z^2} + \frac{1}{R^4} \frac{\partial^4 u}{\partial \phi^4} + \frac{1}{R^4} \frac{\partial^3 v}{\partial \phi^3} \right] \right] \quad (16)$$

$$L_y = C \left[\frac{1-\nu}{2} \frac{\partial^2 v}{\partial z^2} + \frac{1}{R^2} \frac{\partial^2 v}{\partial \phi^2} - \frac{1}{R^2} \frac{\partial u}{\partial \phi} + \frac{1+\nu}{2R} \frac{\partial^2 w}{\partial \phi \partial z} \right] + D \left[\frac{1-\nu}{2R^2} \frac{\partial^2 v}{\partial z^2} + \frac{1}{R^4} \frac{\partial^2 v}{\partial \phi^2} + \frac{1}{R^4} \frac{\partial^3 u}{\partial \phi^3} + \frac{1}{R^2} \frac{\partial^3 u}{\partial \phi \partial z^2} \right] \quad (17)$$

$$L_z = C \left[\frac{\partial^2 w}{\partial z^2} + \frac{1-\nu}{2R^2} \frac{\partial^2 w}{\partial \phi^2} - \frac{v}{R} \frac{\partial u}{\partial z} + \frac{1+\nu}{2R} \frac{\partial^2 v}{\partial \phi \partial z} \right] \quad (18)$$

3.2. Free Vibration Solutions

The natural frequencies and mode shapes for free vibration of the cylindrical shell may be obtained analytically by assuming a solution to Eqs. (13)-(15) in the form

$$\begin{aligned} u &= \alpha e^{\lambda z} \cos(m\phi + \omega t), \\ v &= -\beta e^{\lambda z} \sin(m\phi + \omega t), \\ w &= \gamma e^{\lambda z} \cos(m\phi + \omega t) \end{aligned} \quad (19)$$

with integer value m . For the case with $\Omega = 0$, substituting Eq. (19) in Eqs. (13)–(15), yields

$$\begin{bmatrix} a_4 \lambda^4 + a_2 \lambda^2 + a_0 + a_\omega \omega^2 & d_2 \lambda^2 + d_0 & e_1 \lambda \\ d_2 \lambda^2 + d_0 & b_2 \lambda^2 + b_0 + b_\omega \omega^2 & f_1 \lambda \\ -e_1 \lambda & -f_1 \lambda & c_2 \lambda^2 + c_0 + c_\omega \omega^2 \end{bmatrix} \times \begin{bmatrix} \alpha \\ \beta \\ \gamma \end{bmatrix} = 0 \quad (20)$$

where the coefficient values are given in the appendix. Using a given (assumed) natural frequency value ω allows Eq. (20) to be solved by setting the determinant of the matrix to zero. This gives eight solutions for λ and eight corresponding solutions for (α, β, γ) . The z -dependent mode-shape functions are then given by

$$\begin{aligned} U(z) &= \sum_{i=1}^8 C_i \alpha_i e^{\lambda_i z}, & V(z) &= \sum_{i=1}^8 C_i \beta_i e^{\lambda_i z}, \\ W(z) &= \sum_{i=1}^8 C_i \gamma_i e^{\lambda_i z} \end{aligned} \quad (21)$$

A correct natural frequency value ω is that which (through some choice of coefficients C_i) allows the boundary conditions to be exactly satisfied. For a cylindrical shell with free ends, the boundary conditions are [22]

$$\begin{aligned} \frac{\partial w}{\partial z} + v \left(\frac{\partial v}{\partial \phi} - u \right) \Big|_{z=\pm L/2} &= 0, \\ \frac{\partial^2 u}{\partial z^2} + \frac{v}{R^2} \left(\frac{\partial^2 u}{\partial \phi^2} + \frac{\partial v}{\partial \phi} \right) \Big|_{z=\pm L/2} &= 0, \\ \frac{1}{R^2} \frac{\partial^2 v}{\partial \phi \partial z} + \frac{2-\nu}{R^2} \frac{\partial^3 u}{\partial \phi^2 \partial z} + \frac{\partial^3 u}{\partial z^3} \Big|_{z=\pm L/2} &= 0, \\ \frac{\partial v}{\partial z} + \frac{1}{R} \frac{\partial w}{\partial \phi} + \frac{h^2}{12R^2} \left(\frac{\partial v}{\partial z} + 2 \frac{\partial^2 u}{\partial \phi \partial z} \right) \Big|_{z=\pm L/2} &= 0. \end{aligned} \quad (22)$$

A general (numerical) approach involves performing a direct search over a range of possible natural frequency values. Care must be taken to avoid numerical errors and conditioning problems. Successful application of this procedure is described in the literature [21], [23] and is not elaborated further here.

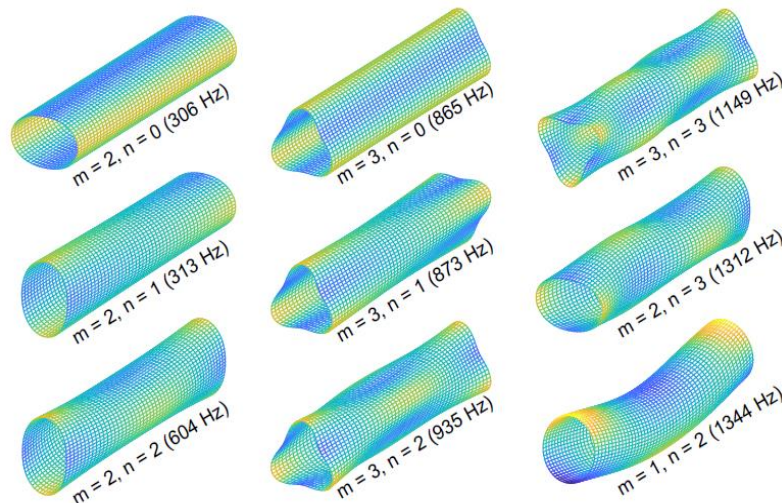


Fig. 4. Rotor mode shapes and natural frequencies for first 9 flexural modes.

Subsequently, the notation $U_{mn}(z)$, $V_{mn}(z)$, and $W_{mn}(z)$ is adopted for the z -dependent mode-shape functions. To identify a given mode, two indices are used: m is the circumferential wavenumber, and n is equal to the number of nodes (zero-crossings) of $U_{mn}(z)$. Free vibration with natural frequency ω_{mn} can be expressed as a summation of two degenerate modes:

$$\begin{bmatrix} u_{mn}(\phi, z, t) \\ v_{mn}(\phi, z, t) \\ w_{mn}(\phi, z, t) \end{bmatrix} = \mathbf{H}_m^p(\phi) \mathbf{G}_{mn}(z) P \cos \omega_{mn} t + \mathbf{H}_m^q(\phi) \mathbf{G}_{mn}(z) Q \sin \omega_{mn} t \quad (23)$$

where $\mathbf{G}_{mn}(z) = [U_{mn}(z) V_{mn}(z) W_{mn}(z)]^T$, and the two circumferential waveforms are out-of-phase by a quarter wavelength:

$$\begin{aligned} \mathbf{H}_m^p(\phi) &= \text{diag}(\sin m\phi, \cos m\phi, \sin m\phi), \\ \mathbf{H}_m^q(\phi) &= \text{diag}(\cos m\phi, -\sin m\phi, \cos m\phi). \end{aligned}$$

The natural frequencies and mode shapes, calculated for the described rotor system, are shown in Fig. 4. The plots show the first eight low frequency wall-flexure modes and first beam bending mode (1344 Hz).

3.3. Parametric Model for Piezo-Actuated Rotor

The general solution for forced vibration may be expressed as a superposition of the free vibration modes:

$$\begin{bmatrix} u_{mn}(\phi, z, t) \\ v_{mn}(\phi, z, t) \\ w_{mn}(\phi, z, t) \end{bmatrix} = \sum_{m=1}^M \sum_{n=1}^N \mathbf{H}_m^p(\phi) \mathbf{G}_{mn}(z) p_{mn}(t) + \mathbf{H}_m^q(\phi) \mathbf{G}_{mn}(z) q_{mn}(t) \quad (24)$$

where $p_{mn}(t)$ and $q_{mn}(t)$ form the set of modal response variables. Substituting in Eqs. (13)-(15), pre-multiplying by $\begin{bmatrix} \mathbf{G}_{mn}^T(z) \mathbf{H}_m^p(\phi) \\ \mathbf{G}_{mn}^T(z) \mathbf{H}_m^q(\phi) \end{bmatrix}$ and integrating over $\phi \in (0, 2\pi]$ and $z \in \left(-\frac{L}{2}, \frac{L}{2}\right)$ yields

$$\begin{aligned} \begin{bmatrix} \ddot{p}_{mn} \\ \ddot{q}_{mn} \end{bmatrix} + \left(\mathbf{D}_{mn} + 2\Omega \frac{b_{mn}}{a_{mn}} \begin{bmatrix} 0 & -1 \\ 1 & 0 \end{bmatrix} \right) \begin{bmatrix} \dot{p}_{mn} \\ \dot{q}_{mn} \end{bmatrix} \\ + \left(\omega_{mn}^2 - \Omega^2 \left(m^2 - \frac{c_{mn}}{a_{mn}} + 2m \frac{b_{mn}}{a_{mn}} \right) \right) \begin{bmatrix} p_{mn} \\ q_{mn} \end{bmatrix} \\ = \frac{1}{\mu_{mn}} \begin{bmatrix} f_p(t) \\ f_q(t) \end{bmatrix} \end{aligned} \quad (25)$$

where the orthogonality properties of the mode shapes must be exploited to obtain

$$\begin{aligned} a_{mn} &= \int_{-\frac{L}{2}}^{\frac{L}{2}} \mathbf{G}_{mn}^T \mathbf{G}_{mn} dz, \\ b_{mn} &= 2 \int_{-\frac{L}{2}}^{\frac{L}{2}} U_{mn} V_{mn} dz, \\ c_{mn} &= 2 \int_{-\frac{L}{2}}^{\frac{L}{2}} (U_{mn} + mV_{mn})^2 dz \end{aligned}$$

Also, $\mu_{mn} = \rho \pi R h a_{mn}$ and \mathbf{D}_{mn} is a diagonal positive definite damping matrix that will be set to match the

experimentally determined damping levels for each mode (as in ref. [21]). The piezo actuation forcing terms are

$$f_{p,q}(t) = e(t) \iint \mathbf{G}_{mn}(z)^T \mathbf{H}_m^{p,q}(\theta) \frac{h}{2} \begin{bmatrix} \frac{K_y}{R^2} \frac{\partial^2 H}{\partial \phi^2} + K_z \frac{\partial^2 H}{\partial z^2} \\ -\frac{K_y}{R^2} \frac{\partial H}{\partial \phi} \\ 0 \end{bmatrix} dz d\phi. \quad (26)$$

Substituting for H using Eq. (7) and integrating by parts gives

$$\begin{aligned} f_p(t) &= \sin m\phi_i E(z_i) e(t), \\ f_q(t) &= \cos m\phi_i E(z_i) e(t). \end{aligned} \quad (27)$$

where the z -dependent coupling coefficient is

$$E(z_i) = \frac{h \sin(mb/R)}{m} \left[K_z [U'(z_i + a) - U'(z_i - a)] - \frac{K_y}{R^2} \int_{z_i-a}^{z_i+a} m^2 U(z) + mV(z) dz \right] \quad (28)$$

The full set of uncoupled modal response equations in the form of Eq. (26), together with Eq. (28), provide a (rotating-frame) multi-mode model for flexural vibration of the piezo-actuated rotor. For piezo patch sensors on the surface of the rotor, the output voltage is proportional to the surface strain:

$$y_j \propto \left[K_z \left(\frac{\partial^2 u}{\partial z^2} \right) + \frac{K_y}{R^2} \left(\frac{\partial^2 u}{\partial \phi^2} + \frac{\partial v}{\partial \phi} \right) \right] \quad (29)$$

Consequently, the amplified output voltage can be expressed

$$y_j(t) = K_{\text{sens}} E(z_j) \sum_{n,m} [\sin m\phi_j \cos m\phi_j] \begin{bmatrix} p_{mn}(t) \\ q_{mn}(t) \end{bmatrix} \quad (30)$$

Table 3. System natural frequencies and damping ($\Omega = 0$).

Mode shape indices	ω_{mn} (Hz) Theoretical	ω_{mn} (Hz) Experiment	ζ_{mn} Experiment
$m = 2, n = 0$	306	304	3.82e-4
$m = 2, n = 1$	313	309	6.15e-4
$m = 2, n = 2$	604	596	5.24e-4
$m = 2, n = 3$	1312	1301	3.75e-4
$m = 3, n = 0$	865	863	6.61e-4
$m = 3, n = 1$	873	870	4.36e-4
$m = 3, n = 2$	935	931	3.82e-4
$m = 3, n = 3$	1149	1140	3.91e-4
$m = 3, n = 4$	1564	1550	4.32e-4
$m = 4, n = 0$	1658	1652	1.05e-4
$m = 4, n = 1$	1665	1663	2.47e-4
$m = 4, n = 2$	1704	1702	1.95e-4
$m = 4, n = 3$	1793	1786	2.11e-4
$m = 4, n = 4$	1963	1949	2.68e-4

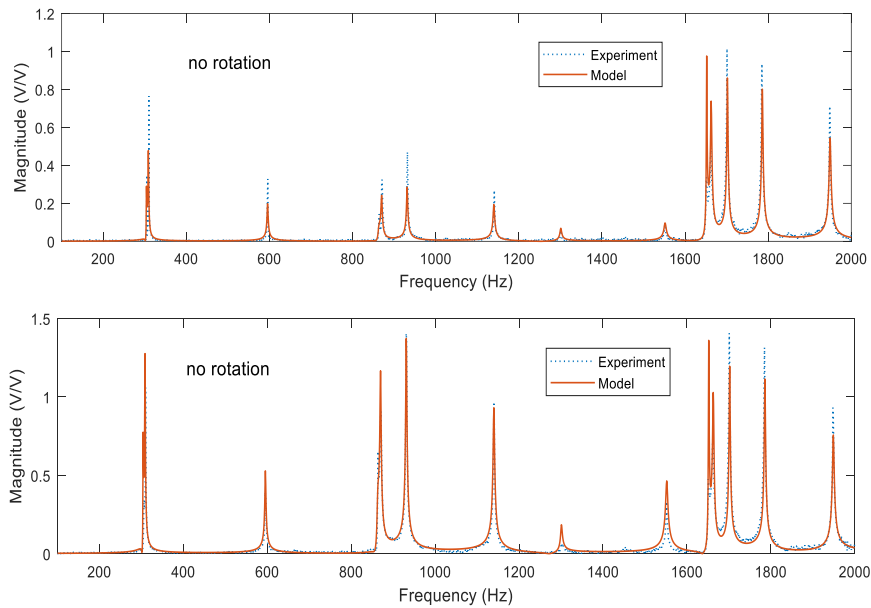


Fig. 5. Measured frequency response of rotor from u_4 to y_1 and u_4 to y_2 for cases without rotation: $\Omega/2\pi = 0$ Hz. Theoretical data for reduced order system model is also shown.

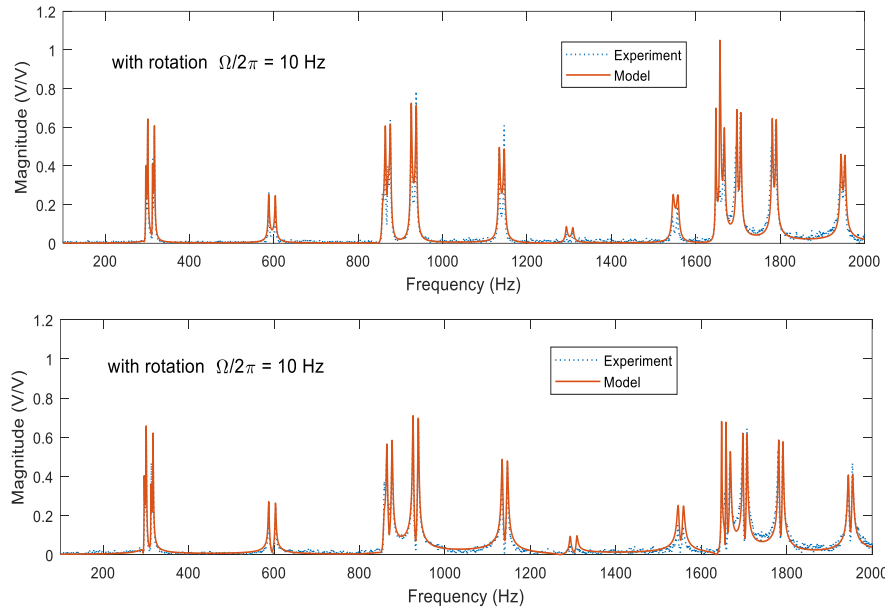


Fig. 6. Measured frequency response of rotor from u_4 to y_1 and u_4 to y_2 for cases with $\Omega/2\pi = 10$ Hz. Theoretical data for reduced order system model is also shown.

3.4. Model Verification and Parameter Updating

The model Eqs. (26)–(30) were used to obtain frequency response data relating actuator input voltages to sensor output voltages. The adopted model included the first 14 pairs of flexural modes (within frequency range 300–2000 Hz). Note that the rigid body modes ($m = 1, n = 0, 1$) do not couple with the piezo transducers and so the corresponding states were omitted. Experimental frequency response data was obtained by applying a sinusoidal excitation voltage to a single piezo patch actuator (u_4). Response measurements are presented for the piezo patch sensors y_1 and y_2 . The experimental and theoretical results for cases without rotation and with rotation at 10 Hz are shown in Fig. 5 and Fig. 6, respectively. Non-collocated input/outputs

were selected to avoid crosstalk between the actuator and sensors. To obtain this high level of agreement, the natural frequencies ω_{mn} and damping ratios ζ_{mn} for the theoretical model were updated to match experimentally identified values, as shown in Table 3. The values of \mathbf{D}_{mn} and ω_{mn} in Eq. (25) were adjusted manually so that all the resonance peaks in the theoretical frequency response matched with the experimental data (with rotation) as closely as possible. It was found that the theoretical values of ω_{mn} were all slightly higher than the experimental values. This can be attributed to the added mass from the patches and electrical wiring. The updated theoretical model correctly predicts the splitting of natural frequencies for forward and backward wave modes (see Fig. 6). This occurs for non-zero rotational speed due to Coriolis forces [21]. Clearly, the

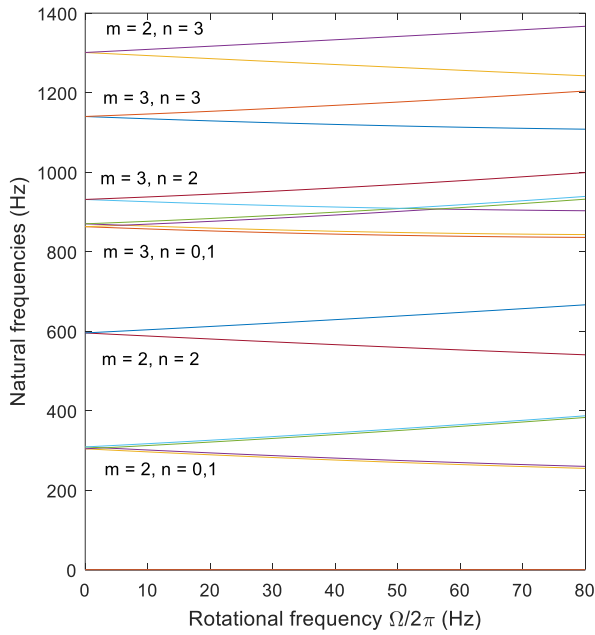


Fig. 7. Campbell diagram for flexural vibration modes of thin-walled rotor system.

speed-dependent dynamics of the rotating cylindrical shell must be accounted for correctly in the model-based controller design. The variation in natural frequencies with rotational speed can be calculated directly from Eq. (25) and depends on the mode-shape coefficients a_{mn} , b_{mn} and c_{mn} . The corresponding Campbell diagram is shown in Figure 7. This aspect was investigated and verified in the study [21]. The results suggest that, in principle, the model and control methodology described here could be applied over a wider range of rotational speeds.

4. Vibration Control Experiments

4.1. Optimal \mathcal{H}_2 Feedback Controller Design

To assess the vibration control capabilities of the piezoelectrics, a feedback controller design was undertaken based on a state-space description of the flexural dynamics, in the form

$$\begin{aligned}\dot{\mathbf{x}} &= \mathbf{A}\mathbf{x} + \mathbf{B}(\mathbf{u} + \mathbf{d}), \\ \mathbf{y} &= \mathbf{C}\mathbf{x} + \mathbf{n},\end{aligned}$$

The matrices \mathbf{A} , \mathbf{B} and \mathbf{C} are obtained directly from Eqs. (26)–(30) by defining a state vector \mathbf{x} that includes the reduced set of modal response variables (\dot{p}_{mn} , \dot{q}_{mn} , p_{mn} , q_{mn}). The control inputs are the set of actuator voltages $\mathbf{u} = [e_1 \ e_2 \ e_3 \ e_4]^T$ and the outputs are the sensor voltages $\mathbf{y} = [y_1 \ y_2 \ y_3 \ y_4]^T$. Process disturbances and sensor noise are represented by additive perturbations, \mathbf{d} and \mathbf{n} , acting on the system inputs and outputs respectively.

To achieve active damping of multiple modes, a cost function is defined based on the \mathcal{H}_2 norm of the closed loop system. The \mathcal{H}_2 norm allows the minimization of

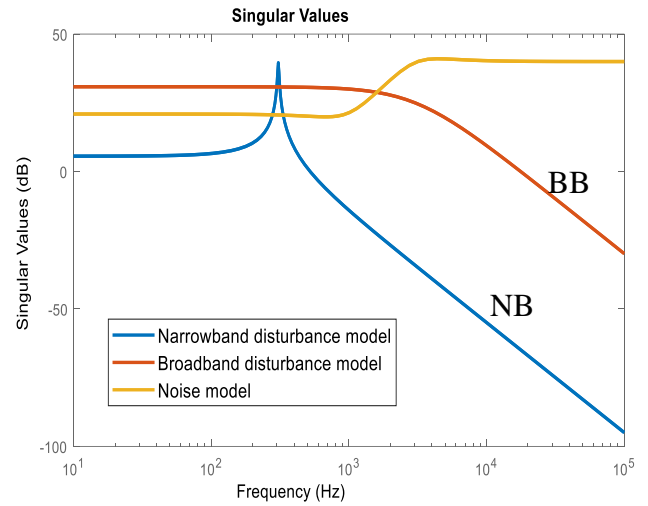


Fig. 8. Singular value plots for disturbance and noise weighting transfer functions (\mathbf{W}_d and \mathbf{W}_n respectively).

the “area” below the frequency response curves, and so can be adopted in order to suppress resonance over a specified bandwidth for control. In this framework, the problem is to obtain a controller $\mathbf{K}_c = \mathbf{C}_c(s\mathbf{I} - \mathbf{A})^{-1}\mathbf{B}_c + \mathbf{D}_c$ that minimizes the \mathcal{H}_2 cost function [24]:

$$J^* = \min_{\mathbf{K}_c} \left\| \begin{bmatrix} \mathbf{T}_{yd}\mathbf{W}_d & \mathbf{T}_{yn}\mathbf{W}_n \\ \epsilon\mathbf{T}_{ud}\mathbf{W}_d & \epsilon\mathbf{T}_{un}\mathbf{W}_n \end{bmatrix} \right\|_2^2, \quad (31)$$

Here, the closed loop transfer function matrices are $\mathbf{T}_{yd} = \mathbf{G}(\mathbf{I} - \mathbf{K}_c\mathbf{G})^{-1}$, $\mathbf{T}_{yn} = \mathbf{G}(\mathbf{I} - \mathbf{K}_c\mathbf{G})^{-1}\mathbf{K}_c$, $\mathbf{T}_{ud} = (\mathbf{I} - \mathbf{K}_c\mathbf{G})^{-1}\mathbf{K}_c\mathbf{G}$, $\mathbf{T}_{un} = (\mathbf{I} - \mathbf{K}_c\mathbf{G})^{-1}\mathbf{K}_c$, where $\mathbf{G}(s) = \mathbf{C}(\mathbf{I}s - \mathbf{A})^{-1}\mathbf{B}$ is the open loop transfer function matrix. The weighting transfer functions \mathbf{W}_d and \mathbf{W}_n are chosen to reflect the spectral characteristics of disturbance and sensor noise, respectively.

The optimal \mathcal{H}_2 control solution then has the property that it achieved the minimum 2-norm (energy) of the weighted output variables $[\mathbf{y}^T \ \epsilon\mathbf{u}^T]^T$. The scalar parameter $\epsilon > 0$ affects the bandwidth of the controller solution and should be chosen to prevent high frequency controller dynamics that might introduce noise and instability problems when applied to the real system, i.e. spillover [25]. The optimal solution for \mathbf{K}_c can be computed from the Riccati equations for separate state estimation and full information control problems [24].

4.2. Controller Test Results

Controllers were synthesized for application with two actuators (inputs e_1 and e_2) and two sensors (outputs y_1 and y_2), having the locations shown in Table 2. Two cases with different input disturbance models \mathbf{W}_d having broadband and narrowband weighting characteristics (see Fig. 8) were considered. The broadband disturbance model was chosen to target circumferential vibration in the frequency range 0-1000 Hz, which involves circumferential modes with $m = 2, 3$ and $n = 0, 1, 2$. The narrowband disturbance model was

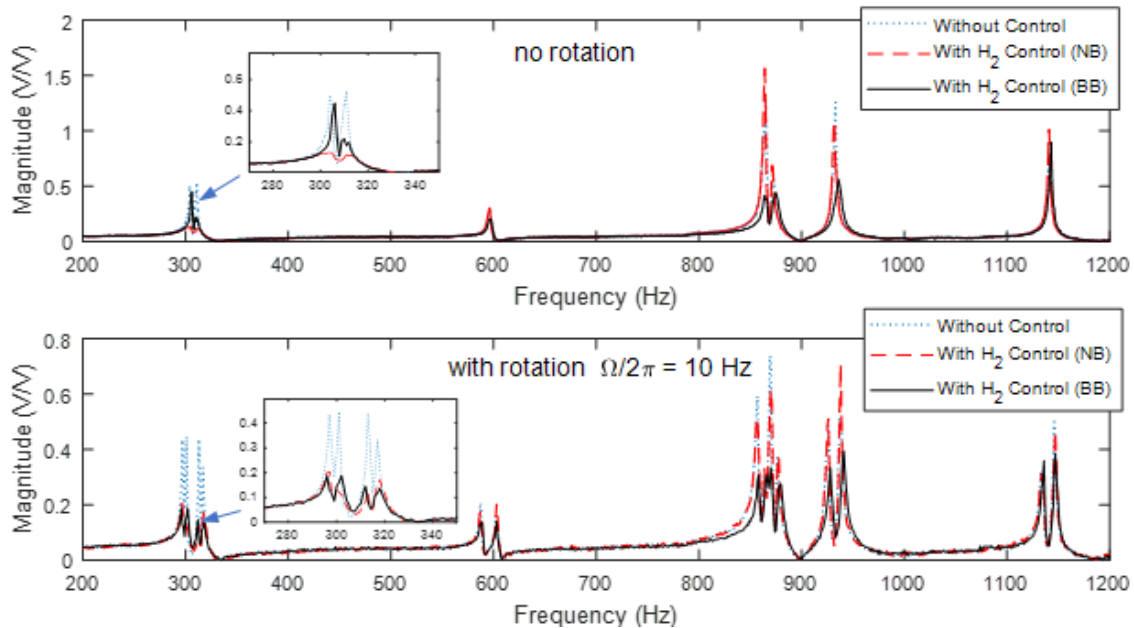


Fig. 9. Measured system frequency response from d_1 to y_1 with feedback control. Controller designs are for narrowband (NB) and broadband (BB) control.

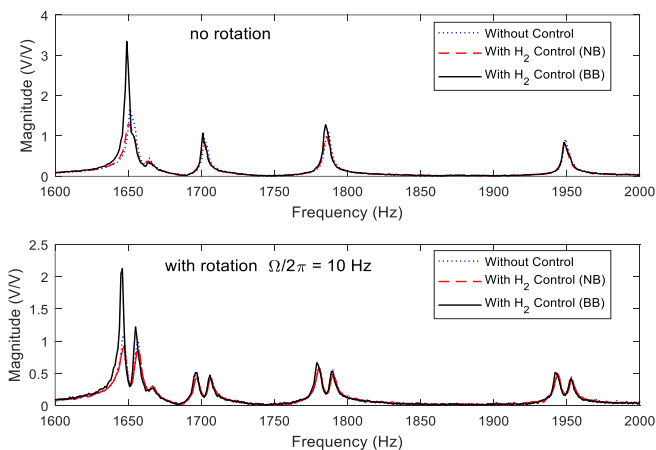


Fig. 10. Measured system frequency response from d_1 to y_1 with feedback control. Some high frequency modes not included in the system model exhibit amplification due to spillover.

chosen to target the lowest frequency circumferential modes ($m = 2, n = 0$ and $m = 2, n = 1$) with natural frequencies close to 300 Hz. The same noise model was adopted for both cases (see Figure 8). The model used for synthesis included all flexural modes up to 1400 Hz and therefore had 32 states.

The frequency response data, with and without control, is given in Fig. 9 and Fig. 10. These graphs show results from the same FRF test but for a low (<1200 Hz) and high (>1600 Hz) frequency range, respectively. The results confirm that flexural vibration can be reduced by the piezo-patch transducers. With use of the broadband disturbance model in the controller synthesis, suppression for elastic modes in the target domain could be achieved. However, amplification of resonance was prone to occur in the high frequency domain (>1400 Hz) caused by spillover problems, as these modes were not included in the model (see Fig. 10). Use of the

narrowband disturbance model allowed efficient suppression of targeted elastic modes without spillover problems.

It is possible that, for the broadband controller, including higher frequency modes (>1400 Hz) in the model could help to avoid their destabilization. However, the controller would then be higher order and so could not be implemented with the high sampling frequency that is required to maintain control bandwidth and prevent phase lag that tends to destabilize high frequency modes, even when they are included in the model. As general practice, it is recommended to omit modes that fall in a frequency range that cannot be modelled sufficiently accurately for controller design purposes.

5. Conclusions

From this study, the following conclusions can be made concerning the application of piezo-based vibration control with a thin-walled rotor:

1. The assumption that only the applied moments from the actuator patches need by considered appears satisfactory for modelling and control of low frequency wall bending modes (i.e. a surface-mounted unimorph patch has a similar control action as a bimorph bending actuator).
2. As the mass and stiffness of the patches were neglected in the structural model, an improved model could be obtained by calibrating the natural frequencies and damping ratios to match experimental results.
3. For the AMB-supported rotor, the effect of bearing stiffness on the flexural mode dynamics could be neglected in the initial model. For higher stiffness bearing types, the impact on the shell dynamics may require more explicit consideration.
4. For the \mathcal{H}_2 control approach, careful selection of weighting functions is required to ensure closed loop

stability even if accurate models are available as errors from order-reduction arise prior to synthesis.

Acknowledgement

This work was supported by the Thailand Research Fund under grant [RGU6280014].

References

- [1] H. G. Horst and H. P. Wolfel, "Active vibration control of a high speed rotor using PZT patches on the shaft surface," *Journal of Intelligent Material Systems and Structures*, vol. 15, pp. 721–732, 2004
- [2] A. W. Lees and M. I. Friswell, "Active balancing of flexible rotors using strain actuators," *Journal of Vibration Engineering and Technologies*, vol. 4, no.6, pp. 483-489, 2016.
- [3] P. J. Sloetjes and A. D. Boer, "Vibration reduction and power generation with piezoceramic sheets mounted to a flexible shaft," *Journal of Intelligent Material Systems and Structures*, vol. 19, pp. 25–34, 2008.
- [4] P. Cupial and M. Koziol, "The analysis of a smart Jeffcott rotor with direct velocity feedback control in the supercritical range," *Journal of Low Frequency Noise, Vibration and Active Control*, vol. 32, no. 3, pp. 205-216, 2013.
- [5] M. Koziol and P. Cupial, "The influence of the active control of internal damping on the stability of a cantilever rotor with a disc," *Mechanics Based Design of Structures and Machines*, pp. 1–14, 2020.
- [6] P. M. Przybyłowicz, "Active stabilization of a rotating shaft transmitting static torque," *Meccanica*, vol. 38, pp. 763–770, 2003.
- [7] M. K. Kwak, S. Heo, and M. Jeong, "Dynamic modelling and active vibration controller design for a cylindrical shell equipped with piezoelectric sensors and actuators," *Journal of Sound and Vibration*, vol. 321, pp. 510–524, 2009.
- [8] M. C. Ray and J. N. Reddy, "Active control of laminated cylindrical shells using piezoelectric fiber reinforced composites," *Composites Science and Technology*, vol. 65, no. 5, pp. 1226–1236, 2005.
- [9] G. Caner, "Active vibration control of beams and cylindrical structures using piezoelectric patches," PhD thesis, Middle East Technical University, 2014.
- [10] J. Plattenburg, J. T. Dreyer, and R. Singh, "Vibration control of a cylindrical shell with concurrent active piezoelectric patches and passive cardboard liner," *Mechanical systems and signal processing*, vol. 91, pp. 422–437, 2017.
- [11] A. Lohmani, M. Danesh, M. K. Kwak, and M. Keshmiri, "Vibration suppression of a piezo-equipped cylindrical shell in a broad-band frequency domain," *Journal of Sound and Vibration*, vol. 411, pp. 260–277, 2017.
- [12] M. Biglar, H. R. Mirdamadi, and M. Danesh, "Optimal locations and orientations of piezoelectric transducers on cylindrical shell based on gramians of contributed and undesired Rayleigh–Ritz modes using genetic algorithm," *Journal of Sound and Vibration*, vol. 333, 2014, pp. 1224-1244.
- [13] K. M. Hu and H. Li, "Multi-parameter optimization of piezoelectric actuators for multi-mode active vibration control of cylindrical shells," *Journal of Sound and Vibration*, vol. 426, pp. 166–185, 2018.
- [14] S. M. Hasheminejad and A. Oveisi, "Active vibration control of an arbitrary thick smart cylindrical panel with optimally placed piezoelectric sensor/actuator pairs," *International Journal of Mechanics and Materials in Design*, vol. 12, pp. 1–16, 2015.
- [15] A. Kumar and M. C. Ray, "Control of smart rotating laminated composite truncated conical shell using ACLD treatment," *International Journal of Mechanical Sciences*, vol. 89, no. 1, pp. 123–141, 2014.
- [16] M. O. T. Cole and W. Fackaew, "An active magnetic bearing for thinwalled rotors: vibrational dynamics and stabilizing control," *IEEE/ASME Transactions on Mechatronics*, vol. 23, pp. 2859–2869, 2018.
- [17] C. Chamroon, M. O. T. Cole, and W. Fackaew, "Model and control system development for a distributed actuation magnetic bearing and thin-walled rotor subject to noncircularity," *ASME Journal of Vibration and Acoustics*, vol. 141, pp. 051006–1, 2019.
- [18] Z. Brand and M. O. T. Cole, "Results on active damping control of a thin-walled rotating cylinder with piezoelectric patch actuation and sensing," *Third IEEE Conference on Control Technology and Applications*, Hong Kong, 2019.
- [19] Z. Brand and M. O. T. Cole, "Controllability and actuator placement optimization for active damping of a thin rotating ring with piezo-patch transducers," *Journal of Sound and Vibration*, vol. 472, p. 115172, 2020.
- [20] A. E. H. Love, *A Treatise on the Mathematical Theory of Elasticity*, 4 ed. Dover Publication, 1944.
- [21] W. Fackaew, M. O. T. Cole, and C. Chamroon, "On the vibrational dynamics of rotating thin-walled cylinders: A theoretical and experimental study utilizing active magnetic bearings," *International Journal of Mechanical Sciences*, vol. 163, p. 105101, 2019.
- [22] W. Soedel, *Vibrations of Shells and Plates*, New York: Marcel Dekker, 2005.
- [23] N. Alujevic, N. Campillo-Davo, P. Kindt, W. Desmet, B. Pluymers, and S. Vercammen, "Analytical solution for free vibrations of rotating cylindrical shells having free boundary conditions," *Engineering Structures*, vol. 132, pp. 152–171, 2017.
- [24] K. Zhou, J. Doyle, and K. Glover, *Robust and Optimal Control*, Pearson, 1995.
- [25] X. Dong, Z. Peng, W. Zhang, H. Hua, and G. Meng, "Research on spillover effects for vibration control of piezoelectric smart structures by ANSYS," *Mathematical Problems in Engineering*, p. 870940, 2014.

APPENDIX - Coefficients of characteristic equation

Defining $\eta = \frac{h^2}{12R^2}$, the coefficients in Eq. (20) may be expressed:

$$a_4 = -\eta R^4, \quad a_2 = 2\eta m^2 R^2, \quad a_0 = -\eta m^4 - 1,$$

$$a_\omega = \frac{\rho h R^2}{c}, \quad b_2 = \frac{1-\nu}{2}(1 + \eta)R^2,$$

$$b_0 = -(1 + \eta)m^2, \quad b_\omega = \frac{\rho h R^2}{c}, \quad c_2 = R^2,$$

$$c_0 = -\frac{1-\nu}{2}m^2, \quad c_\omega = \frac{\rho h R^2}{c},$$

$$d_2 = \eta m R^2, \quad d_0 = -\eta m^3 - m,$$

$$e_1 = \nu R, \quad f_1 = \frac{1+\nu}{2}mR,$$



Ziv Brand was born in Tel Aviv, Israel in 1974. He received his B.Eng. degree in Electrical Engineering from the Negev Academic College in 2003. He then studied at the Ben-Gurion University, receiving the M.Sc. degree in Mechatronics Engineering in 2008. From 2018 he has been a visiting researcher at Chiang Mai University in the Department of Mechanical Engineering, and is currently working toward a Ph.D. degree. Mr Brand's research focuses on the dynamics and control of machine systems, including machining vibration, rotating machinery, magnetic bearings and active vibration control systems.



Matthew O.T. Cole was born in Leamington Spa, England in 1971. After completing his first degree in natural sciences at the University of Cambridge in 1994, he studied at the University of Bath, receiving M.Sc. and Ph.D. degrees in mechanical engineering in 1995 and 1999 respectively. From 2003 he has been a faculty member at Chiang Mai University and is currently a Professor in the Department of Mechanical Engineering. Dr Cole's research interests focus on the dynamics and control of machine systems, including rotating machinery, magnetic bearings and high precision robotics.



Wichaphon Fakkaew was born in Phayao, Thailand in 1977. He received his B. Eng. and M. Eng. Degree from the Department of Mechanical Engineering, Chiang Mai University in 2000 and 2005 respectively. He completed his Ph.D. degree at Chiang Mai University in 2015 and is currently an Assistant Professor in the School of Engineering, University of Phayao. Dr. Fakkaew's research interests include mechanical system modeling and control system design.



Chakkapong Chamroon was born in Phrae, Thailand in 1981. He received his B. Eng. M. Eng. degrees in Mechanical Engineering from Chiang Mai University in 2004 and 2008, respectively, and the Ph.D. degree in 2014 from Chiang Mai University. He was a faculty member at University of Phayao from 2014 to 2019. Since 2020, he has been a faculty member at Chiang Mai University in the Department of Mechanical Engineering. Dr Chamroon's current research interests include dynamics of rotating machinery, vibration control and active magnetic bearing.